Supplementary Materials

Preliminary Study on the Heterogeneous Nucleation Behavior and Interfacial Mechanism of Lysozyme Regulated by Silica Nanoparticles

Qihang Chen, Xiujian Cui and Xiangyang Zhang *

State Key Laboratory of Chemical Engineering, East China University of Science and Technology, Shanghai 200237, China; y82230011@mail.ecust.edu.cn (Q.C.); cxj313905@163.com (X.C.)
* Correspondence: zxydcom@ecust.edu.cn

1 Details of Experiments

It should be noted that the present crystallization system is based on NaCl as the precipitant. In other commonly used systems, such as ammonium sulfate or polyethylene glycol (PEG), the crystallization mechanism may differ due to variations in salting-out effects, excluded volume interactions, and protein–solvent interactions. For example, sulfate salts typically promote crystallization through strong salting-out effects, whereas PEG induces macromolecular crowding. These differences may influence the interaction between proteins and SNP surfaces and consequently affect nucleation behavior. In addition, the presence of divalent cations (e.g., Ca^{2+}, Mg^{2+}) may alter the surface properties of SNPs, particularly their Zeta potential, by screening surface charges or inducing ion bridging effects. Such changes may affect electrostatic interactions between SNPs and protein molecules, thereby influencing protein adsorption and interfacial assembly. Therefore, the nucleation activity of SNPs may be sensitive to solution composition and ionic environment.

Table S1. Summary of HEWL crystallization conditions.

HEWL concentration ($mg \cdot mL^{-1}$)	Buffer species	Buffer concentration (mM)	Buffer pH	Precipitant concentration	Reference
15	CH_3COONa	20	4.8	0.5-1 M	[1]
20	CH_3COONa	100	4.5	0.5-1.5 M	[2]
20	Tris-HCl	20	7.5	0.5 M	[3]
30	CH_3COONa	100	4.6	0.5-1.0 M	[4]

30	CH_3COONa	100	4.6	0.34 M	[5]
30	CH_3COONa	100	4.8	1.1 M	[6]
30	CH_3COONa	100	4.75	3% (wt)	[7]
30	CH_3COONa	100	4.5	4% (wt)	[8]
40	CH_3COONa	100	4.6	0.6 M	[9]
50	CH_3COONa	80	4.8	6.4% (w/v)	[10]

Table S2. Effect of precipitant concentration on HEWL crystallization in the absence and presence of silica nanoparticles.

Additive	Time	NaCl							
		0.3M	0.4M	0.5M	0.6M	0.8M	1.0M	1.2M	1.5M
Without particles	24 h								
	72 h								
80 nm	24 h								
	72 h								
120 nm	24 h								
	72 h								
200 nm	24 h								
	72 h								

, signifies crystal formation; , no solid formation; , amorphous precipitates.

Specific surface areas of SNPs were determined utilizing the Brunauer–Emmett–Teller (BET) method [11]. Measurements were conducted on a Micromeritics ASAP 2460 analyzer.

Prior to analysis, samples were degassed at 150 °C under vacuum to eliminate adsorbed gases. Nitrogen adsorption isotherms were collected at controlled pressures, and the BET equation was applied to calculate the surface area, as given by

$$\frac{P}{V(P_0\text{-}P)} = \frac{1}{V_m C} + \frac{C\text{-}1}{V_m C}\frac{P}{P_0} \quad (1)$$

where V (m^3) represents the volume of the adsorbed gas, V_m ($m^3 \cdot g^{-1}$) is the monolayer adsorption capacity, and C is the adsorption constant. P (Pa) and P_0 (Pa) denote the bulk and saturation pressures of the adsorbed gas, respectively. Using nitrogen adsorption data at various partial pressures, a plot was constructed with the x-axis representing (P/P_0) and the y-axis representing ($P/V(P_0\text{-}P)$) according to Eq. (1) [11, 12]. Through graphical analysis, the values of V_m and C were determined. Given the known cross-sectional area of a nitrogen molecule (A = 0.162 nm^2), the specific surface area (SSA) of silica dioxide was calculated from the V_m value.

2 Simulation Details

To enhance our comprehension of the mechanisms by which silica particles influence HEWL crystallization at the molecular level, we employed simulation software containing AutoDock and Materials Studio (version 2019, Accelrys Software Inc., US) to conduct molecular docking and MD simulations of the HEWL crystallization process. In this research, amorphous silica was synthesized utilizing the Forcite module of the Materials Studio (MS) software. Initially, a supercell of crystalline silica was created, followed by MD simulations conducted at elevated temperatures. The simulations were performed within the NVT ensemble, with the temperature maintained at the melting point of silica (1996 K) for a duration of 1000 ps. Subsequently, a quenching process was executed by lowering the temperature to 298 K under the NVT ensemble, while preserving the same simulation duration of 1000 ps. This heating–quenching cycle was repeated three times to achieve a structure that more accurately reflects experimental conditions. The silica model was developed in accordance with the methodology established by Zhang et al. [13]. Within the framework of the MS Build module, the Nanocluster tool was employed to create spherical silica molecular clusters measuring 10 Å in diameter. This size is considerably smaller than the silica particles used in experimental studies, which typically have a minimum size of 80 nm. However, this choice was made to enhance computational efficiency and cost-effectiveness. Additionally, the existing literature has highlighted the use of 10 Å nanoparticles in molecular docking and MD simulations, thereby reinforcing the validity of this approach [14]. To address the unsaturated boundary effects, hydrogen atoms were introduced to passivate the unsaturated oxygen atoms, while

hydroxyl groups were added to the unsaturated silicon atoms. This process resulted in the formation of spherical silica structures (Figure S1). The silica model was then fully hydrogenated using AutoDock Tools (ADT) software, which also facilitated the analysis of torsional flexibility. Ultimately, the structure was designated as a ligand with an automatic charge distribution, and the output was saved in pdbqt format for subsequent computational studies.

To initiate the process, a suitable protein crystal structure was selected, preferably one derived from X-ray crystallography with high resolution. Following a thorough analysis, hen egg white lysozyme (PDB ID: 1LSF) was identified due to its X-ray resolution of 1.7 Å. The AutoDock Tools (ADT) software was subsequently utilized to preprocess the protein structure by removing water molecules and adding full hydrogen atoms (Figure S2). After completing these modifications, the protein was designated as a macromolecular receptor. At this stage, AutoDock4 (AD4) automatically adjusted the protein's charge and atom types while incorporating non-polar hydrogen atoms, ensuring compatibility for the subsequent molecular docking simulations.

After preparing both the ligand and the receptor, a docking grid box was constructed using ADT. Given that the precise active site of HEWL is not well-defined, the grid box was designed to encompass the entire HEWL molecule with a grid spacing of 108 Å × 98 Å × 112 Å. The docking procedure comprised two fundamental steps. Initially, the AutoGrid program was executed to conduct preliminary calculations. AutoGrid precomputes interaction energy grid maps for various atomic types within the macromolecule, thereby significantly reducing

computational time during the docking process. In the subsequent step, the AutoDock program was utilized to search for and evaluate docking conformations. The Lamarckian Genetic Algorithm (LGA) was employed as the search method due to its high computational accuracy. To ensure optimal conformational sampling, the LGA parameters were configured as follows: the number of independent runs was set to 100, the maximum number of energy evaluations per run was 3×10^6, and the maximum number of random initializations per conformation was set to 3×10^4. Following the docking simulations, the 100 resulting conformations were clustered based on the root-mean-square deviation (RMSD) between the Cartesian coordinates of the ligand atoms. The clusters were then ranked according to binding free energy, and the conformation with the lowest binding free energy was selected as the optimal docking pose. Furthermore, specific HEWL fragments were selected based on known binding sites to conduct MD simulations of the interactions between silica and HEWL. By integrating circular dichroism spectroscopy data with molecular docking simulations, three representative structural motifs of HEWL—including the docking site—were identified: the helical structure, β-sheet structure, and random coil structure. MD simulations of these three HEWL fragments at the silica interface were subsequently conducted to examine the conformational changes induced by silica–HEWL interactions.

The foundational framework for MD simulations was established utilizing the Amorphous Cell module, while geometry optimization and MD simulations were executed through the Forcite module. Taking the SEG 1 fragment as a case study, the initial simulation system consisted of a 10 Å silica spherical cluster, a HEWL fragment (SEG 1), and 100 water

molecules. The system density was calibrated to 0.9970 $g \cdot cm^{-3}$, which aligns with the density of water at 298.15 K. The COMPASS force field was applied, resulting in the generation of 10 structural conformations as output. The conformation exhibiting the lowest total energy (-3198 $kcal \cdot mol^{-1}$) was chosen for subsequent geometric optimization. Following optimization, the structure was annealed using the Forcite-Anneal procedure to obtain the most stable conformation. The annealing cycle temperature ranged from 300 K to 500 K, with 10 cycles performed. After annealing, the lowest-energy conformation (-3240 $kcal \cdot mol^{-1}$) was selected as the initial structure for subsequent MD simulations. The simulations were conducted under the NVT ensemble at a constant temperature of 298.15 K, with a total runtime of 1000 ps. The MD simulation procedures for the SEG 2 and SEG 3 fragments interacting with silica were identical to those applied to SEG 1.

4 Supporting Figures

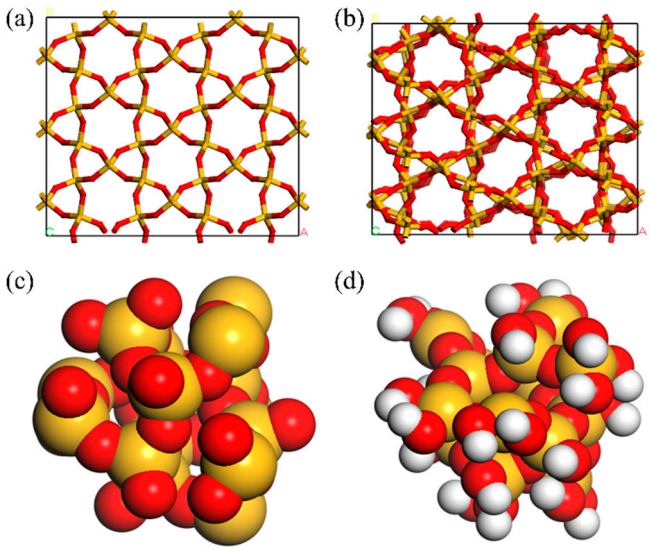


Figure S1. The building of silica model for molecular docking: (a) crystal structure of silica, (b) amorphous silica, (c) spherical silica particles with unsaturated bonds, (d) spherical silica particles terminated by surface atoms.

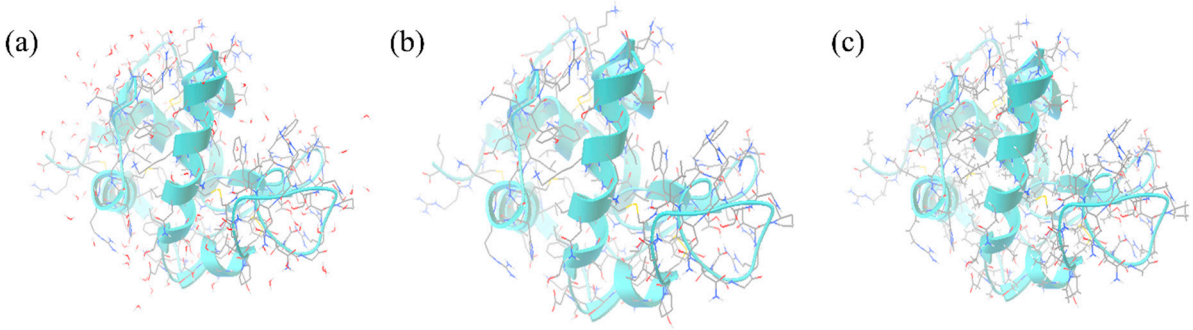


Figure S2. Processing of receptor protein model for molecular docking: (a) crystal structure of HEWL downloaded from PDB database, (b) HEWL structure after removing water molecules, (c) HEWL structure after hydrogenation.

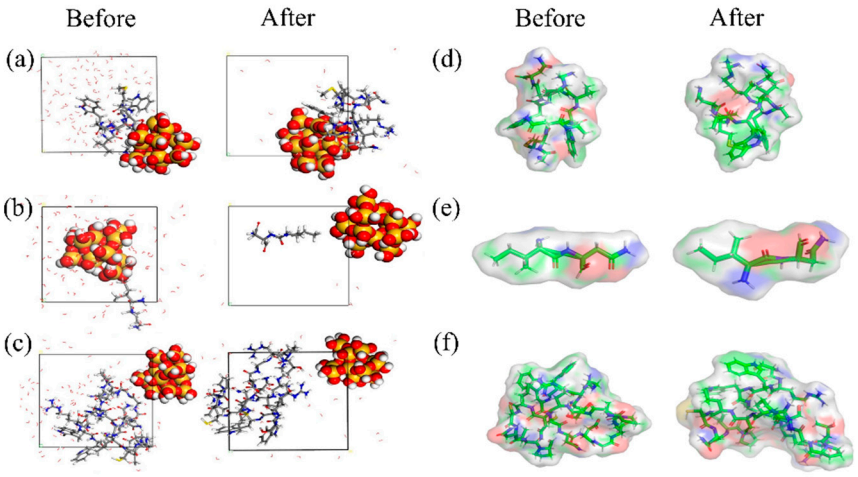


Figure S3. Visual representations of the helical structure and 10 Å silica spherical clusters before and after MD simulations: (a) SEG 1; (b) SEG 2; (c) SEG 3. Surface topological structures of the 10 Å silica spherical clusters before and after MD simulations: (d) SEG 1; (e) SEG 2; (f) SEG 3.

5 References

1. Takeda, Y.; Mafuné, F. Self-assembly of positively charged platinum nanoparticles in lysozyme crystal. *Chem. Phys. Lett.* **2014**, *604*, 110–115.
2. Govada, L.; Leese, H.S.; Saridakis, E.; Kassen, S.; Chain, B.; Khurshid, S.; Menzel, R.; Hu, S.; Shaffer, M.S.; Chayen, N.E. Exploring carbon nanomaterial diversity for nucleation of protein crystals. *Sci. Rep.* **2016**, *6*, 20053.
3. Xing, Y.; Hu, Y.; Jiang, L.; Gao, Z.; Chen, Z.; Chen, Z.; Ren, X. Zwitterion-immobilized imprinted polymers for promoting the crystallization of proteins. *Cryst. Growth Des.* **2015**, *15*, 4932–4937.
4. Liu, Y.-M.; Li, H.-S.; Wu, Z.-Q.; Chen, R.-Q.; Lu, Q.-Q.; Guo, Y.-Z.; Zhang, C.-Y.; Yin, D.-C. Sensitivity of lysozyme crystallization to temperature variation. *CrystEngComm* **2016**, *18*, 1609–1617.
5. Tanaka, S.; Ito, K.; Hayakawa, R.; Ataka, M. Size and number density of precrystalline aggregates in lysozyme crystallization process. *J. Chem. Phys.* **1999**, *111*, 10330–10337.
6. Roberts, M.M.; Heng, J.Y.; Williams, D.R. Protein crystallization by forced flow through glass capillaries: Enhanced lysozyme crystal growth. *Cryst. Growth Des.* **2010**, *10*, 1074–1083.
7. Longo, M.; Heigl, R.; Schrader, T.E. Real-time investigation of Lysozyme crystallization kinetics: A neutron diffraction study. *J. Cryst. Growth* **2021**, *576*, 126362.
8. Yu, X.; Tian, N.; Huang, F.; Huang, X.; Liu, C.; Gao, S.; Yang, Z.; Wu, Y. Evaluating the role of ionic liquids (ILs) in the crystallization of lysozyme. *J. Mol. Liq.* **2019**, *296*, 112018.
9. Gully, B.S.; Zou, J.; Cadby, G.; Passon, D.M.; Iyer, K.S.; Bond, C.S. Colloidal graphenes as heterogeneous additives to enhance protein crystal yield. *Nanoscale* **2012**, *4*, 5321–5324.
10. Tang, L.; Huang, Y.; Liu, D.; Li, J.; Mao, K.; Liu, L.; Cheng, Z.; Gong, W.; Hu, J.; He, J. Effects of the silanized mica surface on protein crystallization. *Acta Crystallogr. Sect. D Biol. Crystallogr.* **2005**, *61*, 53–59.
11. Osterrieth, J.W.; Rampersad, J.; Madden, D.; Rampal, N.; Skoric, L.; Connolly, B.; Allendorf, M.D.; Stavila, V.; Snider, J.L.; Ameloot, R. How reproducible are surface areas calculated from the BET equation? *Adv. Mater.* **2022**, *34*, 2201502.
12. Triantafyllidis, K.S.; Pinnavaia, T.J.; Iosifidis, A.; Pomonis, P.J. Specific surface area and I-point evidence for microporosity in nanostructured MSU-S aluminosilicates assembled from zeolite seeds. *J. Mater. Chem.* **2007**, *17*, 3630–3638.
13. Zhang, Y.; Wang, Y.; Li, Y.; Zhang, Z. The mechanical properties of poly (urea-formaldehyde) incorporated with nano-SiO_2 by molecular dynamics simulation. *Polymers* **2019**, *11*, 1447.
14. Wu, Y.; Zhang, H.; Wang, Y. Conformational and functional changes of bovine serum albumin induced by TiO_2 nanoparticles binding. *J. Mol. Liq.* **2017**, *243*, 358–368.